International Journal of Thermal Sciences 49 (2010) 963–975

Contents lists available at ScienceDirect

International Journal of Thermal Sciences

journal homepage: www.elsevier.com/locate/ijts

Laminar periodic flow and heat transfer in square channel with 45° inline baffles on two opposite walls

Pongjet Promvonge*, Somchai Sripattanapipat, Sutapat Kwankaomeng

Department of Mechanical Engineering, Faculty of Engineering, King Mongkut's Institute of Technology Ladkrabang, Bangkok 10520, Thailand

ARTICLE INFO

Article history:
Received 11 July 2009
Received in revised form
17 November 2009
Accepted 6 January 2010
Available online 4 February 2010

Keywords:
Periodic flow
Square channel
Laminar flow
Heat transfer
Angled baffle

ABSTRACT

A numerical investigation has been carried out to examine laminar flow and heat transfer characteristics in a three-dimensional isothermal wall square channel with 45°-angled baffles. The computations are based on the finite volume method, and the SIMPLE algorithm has been implemented. The fluid flow and heat transfer characteristics are presented for Reynolds numbers based on the hydraulic diameter of the channel ranging from 100 to 1000. To generate a pair of mainstreamwise vortex flows through the tested section, baffles with an attack angle of 45° are mounted in tandem and inline arrangement on the lower and upper walls of the channel. Effects of different baffle heights on heat transfer and pressure loss in the channel are studied and the results of the 45° inline baffle are also compared with those of the 90° transverse baffle and the 45° staggered baffle. It is apparent that in each of the main vortex flows, a pair of streamwise twisted vortex (P-vortex) flows created by the 45° baffle exist and help to induce impinging flows on a sidewall and wall of the baffle cavity leading to drastic increase in heat transfer rate over the channel. In addition, the rise in the baffle height results in the increase in the Nusselt number and friction factor values. The computational results reveal that numerical results of both the 45° inline and staggered baffles are nearly the same. The optimum thermal enhancement factor is at the 45° baffle height of 0.2 times of the channel height for both arrays. The maximum thermal enhancement factor of the 45° baffle in the Re range studied is found to be about 2.6 or twice higher than that of the 90° transverse baffle.

1. Introduction

The need of high performance thermal systems leads to interest in developing techniques for heat transfer enhancement resulting in the reduction of overall heat exchanger dimensions and increasing efficiency. For decades, baffles or ribs have been used in many thermal systems due to their high thermal loads and decreased dimensions. The cooling or heating fluid is supplied into the channels mostly mounted with several ribs/baffles to increase the degree of cooling or heating levels and this configuration is often used in the design of heat exchangers. The use of ribs/baffles completely makes the change of the flow field and thus the distribution of the local heat transfer coefficient. Apart from inducing the mainstream separation, a single transverse rib/baffle can create a recirculation zone ahead of it, a second recirculation zone behind the rib/baffle and a reattachment at the channel wall. In addition, if the rib/baffle is placed at an inclination angle with respect to the axial direction, secondary flows are induced over the channel, resulting in the rise in the heat transfer rate towards the upstream rib/baffle region with respect to the downstream one. Although heat transfer is increased through the rib/baffle arrangement, the pressure drop of the channel flow is also increased due to the decreased flow area effects. Therefore, rib/baffle spacing, angle of attack and height are among the most important parameters used in the design of channel heat exchangers. It is, thus, difficult to realize the advantage of rib/baffle arrangements or geometry. The use of staggered ribs (or transverse baffles) with height and pitch spacing of 0.1 (or 0.5) and 1 times of the channel height respectively is often suggested in most of previous work.

For baffles, the first work on the numerical investigation of flow and heat transfer characteristics in a duct with the concept of periodically fully developed flow was conducted by Patankar et al. [1]. Berner et al. [2] suggested that a laminar behavior for a channel with transverse baffles mounted on two opposite walls is found at a Reynolds number below 600 and for such conditions the flow is free of vortex shedding. Webb and Ramadhyani [3] numerically investigated the fluid flow and heat transfer characteristics in

* Corresponding author. Tel.: +662 3264197; fax: +662 3264198.
E-mail address: kppongje@kmitl.ac.th (P. Promvonge).

1290-0729/$ – see front matter © 2010 Elsevier Masson SAS. All rights reserved.
doi:10.1016/j.ijthermalsci.2010.01.005

Nomenclature

BR	blockage ratio, (b/H)
BLE	baffle leading end
BTE	baffle trailing end
b	baffle height, m
D	hydraulic diameter of square channel, ($=H$)
e	rib height, m
f	friction factor
GCI	grid convergence index
H	channel height, m
h	convective heat transfer coefficient, W m^{-2} K^{-1}
k	thermal conductivity, W m^{-1} K^{-1}
L	cyclic length of one cell (or axial pitch length, H), m
Nu	Nusselt number
P	rib pitch length, m
p	static pressure, Pa
Pr	Prandtl number
Re	Reynolds number, ($\rho\overline{u}D/\mu$)
S_{ij}	rate of strain tensor
s	pitch or spacing ratio, L/H
T	temperature, K
u_i	velocity in x_i-direction, m s^{-1}
$\overline{u}$	mean velocity in channel, m s^{-1}

Greek letter

μ	dynamic viscosity, kg s^{-1} m^{-1}
Γ	thermal diffusivity
Ω_{ij}	vorticity tensor
α	baffle inclination angle or angle of attack, degree
λ_2	secondeigenvalue of symmetric tensor $S_{ij}S_{ji} + \Omega_{ij}\Omega_{ji}$
η	thermal enhancement factor, ($=(Nu/Nu_0)/(f/f_0)^{1/3}$)
ρ	density, kg m^{-3}

Subscript

in	inlet
0	smooth channel
w	wall
pp	pumping power

a smooth channel with staggered baffles, based on the periodically fully developed flow conditions of Patankar et al. [1]. Kellar and Patankar [4] studied the heat transfer behaviors in a channel with staggered baffles and reported that the heat transfer increases with the rise in baffle height and with the decrease in baffle spacing. Their results showed similar behaviors as results of Webb and Ramadhyani [3]. Cheng and Huang [5] investigated the case of asymmetrical baffles and indicated that the friction factor shows a great dependence on baffle location, especially for a large height of baffle. Cheng and Huang [6] again presented laminar forced convection in the entrance region of a horizontal channel with one or two pairs of baffles placed on the walls. Habib et al. [7] reported the characteristics of turbulent flow and heat transfer inside the periodic cell formed between segmented baffles staggered in a rectangular duct and pointed out that the pressure drop increases with the baffle height.

Amiri et al. [8] investigated both experimentally and numerically the laminar flow and heat transfer in a two-dimensional channel with packed bed porous media using a two-phase equation model for the transport. A numerical investigation of laminar forced convection in a three-dimensional channel with baffles for periodically fully developed flow and with a uniform heat flux in the top and bottom walls was conducted by Lopez et al. [9]. Guo and Anand [10] studied the three-dimensional heat transfer in a channel with a single baffle in the entrance region. Numerical studies for both solid and porous baffles in a two-dimensional channel for the turbulent flow [11] and for the laminar flow regimes [12,13] were conducted and similar thermal performance results for both the solid and porous cases were reported. Ko and Anand [14] carried out an experiment for turbulent channel flow with porous baffles and found that the porous baffles present a flow behavior as good as the one with solid baffles. Mousavi and Hooman [15] numerically studied the heat transfer behavior in the entrance region of a channel with staggered baffles for Reynolds numbers ranging from 50 to 500 and baffle heights between 0 and 0.75 and reported that the Prandtl number affects the precise location of the periodically fully developed region. Tsay et al. [16] investigated numerically by using baffles for enhancement of heat transfer in laminar channel flow over two heated blocks mounted on the lower plate. A numerical study of laminar periodic flow and thermal behaviors in a two-dimensional channel fitted with staggered diamond-shaped baffles was performed by Sripattanapipat and Promvonge [17]. They reported that the diamond baffle with half apex angle of 5–10° provided slightly better thermal performance than the flat baffle. Promvonge et al. [18] also investigated numerically the laminar heat transfer enhancement in a square channel with 45 deg inclined baffle mounted on one wall. They found that a single mainstreamwise vortex flow occurs for using the periodic baffles and P-vortex exists and helps to induce impingement jets on the wall of the baffle cavity and the BTE sidewall. The appearance of vortex-induced impingement flows leaded to the thermal enhancement factor of about 2.2 at BR = 0.4 and Re = 1200.

For ribs, many investigations have been carried out to examine the rib parameter effects on heat transfer and friction factor for two opposite roughened surfaces. Han et al. [19,20] studied experimentally the heat transfer in a square channel with different angled rib arrays on two walls for $P/e = 10$ and $e/D = 0.0625$. They reported that the angled ribs and 'V' ribs provided higher heat transfer enhancement than the continuous ribs and the highest value is at the 60° orientation amongst the angled ribs. Liou and Hwang [21,22] investigated the performance of square, triangular and semi-circular ribs using a real time Laser Holographic Interferometry to measure the local as well as average heat transfer coefficients and reported that the square ribs give the best heat transfer performance. Taslim et al. [23] studied the heat transfer behaviors in a ribbed square channel with three e/D ratios ($e/D = 0.083$, 0.125 and 0.167) and a fixed $P/e = 10$ using a liquid crystal technique. The average Nusselt number was increased with the rise in e/D ratio and the best one of the e/D ratios was found to lie between 0.083 and 0.125. Murata and Mochizuki [24] studied numerically the heat transfer distribution in a ribbed square channel with $e/D = 0.1$, $P/e = 10$ and 60° orientation using large eddy simulation and reported that the flow reattachment at the midpoint between ribs caused a significant increase in the local heat transfer.

Chandra et al. [25] carried out measurements on heat transfer and pressure loss in a square channel with continuous ribs and found that the heat transfer augmentation increases with the rise in the number of ribbed walls. Tanda [26] examined the effect of transverse, angled ribs, discrete, angled discrete ribs, V-shaped, V-shaped broken and parallel broken ribs on heat transfer and friction. It was found that 90° transverse ribs provided the lowest thermal performance while the 60° parallel broken ribs or 60° V-shaped broken ribs yielded a higher heat transfer augmentation

than the 45° parallel broken ribs or 45° V-shaped broken ribs. Parallel angled discrete ribs were seen to be superior to parallel angled full ribs and its 60° discrete ribs performed the highest heat transfer. Promvonge and Thianpong [27] studied the thermal performance of wedge ribs, triangular and rectangular ribs mounted on the two opposite walls of a channel and found that the inline wedge rib pointing downstream provides the highest heat transfer but the staggered triangular rib gives the best thermal performance. Comprehensive reviews over hundred references on heat transfer enhancement by periodic surfaces mounted ribs in ducts for both numerical and experimental works were reported by Hans et al. [28] and Varun et al. [29].

Most of the investigations on laminar flow as mentioned earlier have considered the heat transfer characteristics for blockage ratio and spacing ratio values for porous or solid transverse baffles only. Although inclined, V-shaped, continuous or broken ribs cited above have been studied extensively; most of the ribs investigated were based on square cross section or thick ribs only. Therefore, the study on inclined baffles (or ribs with nearly zero thickness) in square channels has rarely been reported. In the present work, the numerical computations for three-dimensional laminar periodic channel flows over a 45° inclined baffle pair mounted on two opposite channel walls are conducted with the main aim being to examine the changes in the flow structure and heat transfer performance. The use of the inline 45° baffles placed periodically over the opposite walls of the tested channel is expected to generate a pair of longitudinal vortex flows through the channel to better mixing of fluid flows between the core and the wall resulting in higher heat transfer rate in the channel.

2. Flow configuration and mathematical foundation

2.1. Baffle geometry and arrangement

The system of interest is a horizontal square channel with a 45° baffle pair placed on the upper and lower channel walls in tandem for both inline and staggered arrangements as shown in Fig. 1. For the staggered arrangement, the upper plate is moved to the right by half the interbaffle spacing and the computational domain and the grid size for both arrangements are similar. The flow under consideration is expected to attain a periodic flow condition in which the velocity field repeats itself from one cell to another. The concept of periodically fully developed flow and its solution procedure has been described in Ref. [1]. The air enters the channel at an inlet temperature, T_{in}, and flows over a 45°-angled baffle pair where b is the baffle height, H set to 0.05 m, is the channel height and b/H is known as the blockage ratio, BR. The axial pitch, L or distance between the baffle cell is set to $L = H$ in which L/H is defined as the pitch ratio, $s = 1$. To investigate an effect of the interaction between baffles, the baffle blockage ratio, BR of both inline and staggered baffle arrays is varied in a range of BR = 0.05–0.3 for $\alpha = 45°$ in the present investigation. Also, a typical transverse baffle ($\alpha = 90°$) is introduced for comparison.

2.2. Mathematical foundation

The numerical model for fluid flow and heat transfer in the square channel was developed under the following assumptions:

- Steady three-dimensional fluid flow and heat transfer.
- The flow is laminar and incompressible.
- Constant fluid properties.
- Body forces and viscous dissipation are ignored.
- Negligible radiation heat transfer.

Based on the above assumptions, the channel flow is governed by the continuity, the Navier–Stokes equations and the energy equation. In the Cartesian tensor system these equations can be written as follows:

Continuity equation:

$$\frac{\partial}{\partial x_i}(\rho u_i) = 0 \tag{1}$$

Momentum equation:

$$\frac{\partial(\rho u_i u_j)}{\partial x_j} = -\frac{\partial p}{\partial x_i} + \frac{\partial}{\partial x_j}\left[\mu\left(\frac{\partial u_i}{\partial x_j} + \frac{\partial u_j}{\partial x_i}\right)\right] \tag{2}$$

Energy equation:

$$\frac{\partial}{\partial x_i}(\rho u_i T) = \frac{\partial}{\partial x_j}\left(\Gamma\frac{\partial T}{\partial x_j}\right) \tag{3}$$

where Γ is the thermal diffusivity and is given by

$$\Gamma = \frac{\mu}{Pr} \tag{4}$$

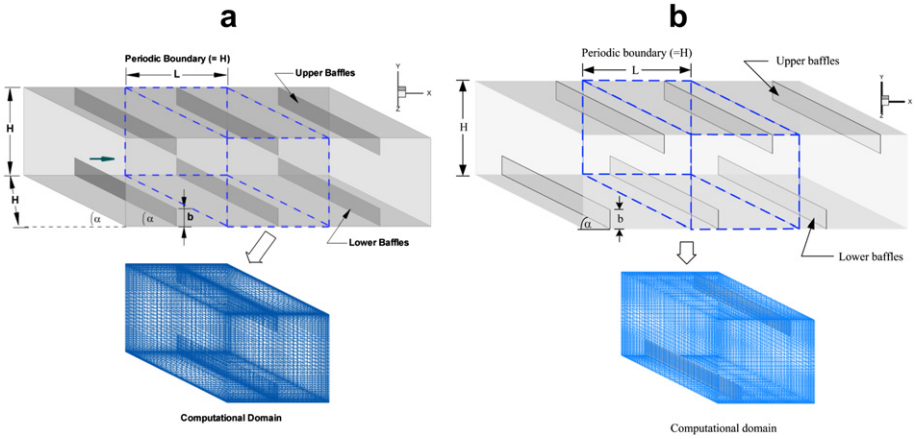

Fig. 1. Channel geometry and computational domain of periodic flow: (a) inline and (b) staggered.

Apart from the energy equation discretized by the QUICK scheme, the governing equations were discretized by the second order upwind differencing scheme, decoupling with the SIMPLE algorithm and solved using a finite volume approach [30]. The solutions were considered to be converged when the normalized residual values were less than 10^{-5} for all variables but less than 10^{-9} only for the energy equation.

Four parameters of interest in the present work are the Reynolds number, friction factor, Nusselt number and thermal enhancement factor. The Reynolds number is defined as

$$Re = \rho \overline{u} D/\mu \tag{5}$$

The friction factor, f is computed by pressure drop, Δp across the length of the periodic channel, L as

$$f = \frac{(\Delta p/L)D}{\frac{1}{2}\rho \overline{u}^2} \tag{6}$$

The heat transfer is measured by local Nusselt number which can be written as

$$Nu_x = \frac{h_x D}{k} \tag{7}$$

The average Nusselt number can be obtained by

$$Nu = \frac{1}{L}\int Nu_x \partial x \tag{8}$$

The thermal enhancement factor (η) is defined as the ratio of the heat transfer coefficient of an augmented surface, h to that of a smooth surface, h_0, at an equal pumping power and given by

$$\eta = \left.\frac{h}{h_0}\right|_{pp} = \left.\frac{Nu}{Nu_0}\right|_{pp} = (Nu/Nu_0)/(f/f_0)^{1/3} \tag{9}$$

where Nu_0 and f_0 stand for Nusselt number and friction factor for the smooth channel, respectively.

For visualization of vortices in three-dimensional flows, the coherent structure detecting method based on the λ_2-criterion of Jeong and Hussain [31] is introduced in the current study. In this method, a vortex is defined as a region where the second eigenvalue, λ_2, of the symmetric tensor $S_{ij}S_{ji} + \Omega_{ij}\Omega_{ji}$ is negative. The tensors S_{ij} and Ω_{ij} are the symmetric and antisymmetric parts of the velocity gradient tensor or called the rate of strain tensor and vorticity tensor, respectively and have the form as follows:

$$S_{ij} = \frac{1}{2}\left(\frac{\partial u_i}{\partial x_j} + \frac{\partial u_j}{\partial x_i}\right) \tag{10}$$

$$\Omega_{ij} = \frac{1}{2}\left(\frac{\partial u_i}{\partial x_j} - \frac{\partial u_j}{\partial x_i}\right) \tag{11}$$

The vortex-core extraction method mentioned above can find lines that run through the center of the region of negative λ_2. A rotating structure can be raised to view as an “iso-surface” of constant λ_2, where $\lambda_2 < 0$ is realized.

The computational domain is resolved by regular Cartesian elements. For this channel flow, however, regular grid was applied throughout the domain. A grid independence procedure was implemented by using Richardson extrapolation technique over grids with different numbers of cells. The characteristics of four grids; 21,600, 41,600, 80,000 and 163,200 cells, used in the simulations are listed in Table 1. In the table, the variation in Nu and f values for the 45° inline baffles at BR = 0.1 and $Re = 500$ is marginal when increasing the number of cells from 80,000 to 163,200, hence there is no such advantage in increasing the number of cells beyond this value. From the values of the parameters it follows that the grid convergence index (GCI) [32,33] can be obtained for different grids as shown in Table 1. GCI represents an estimation of the discretization error between numerical solution, calculated over finer grid and numerical solutions calculated over coarser ones. Because GCI values are almost constant, grid independence condition was obtained. Considering both convergent time and solution precision, the grid system of 80,000 cells was adopted for the current computational model.

Table 1
Grid features.

Grid size	Nu	f	Error (%)		GCI (%)	
			Nu	f	Nu	f
163,200	6.9197	0.3421	0.1155	0.1344	0.0277	0.0214
80,000	6.9277	0.3425	0.5974	0.0123	0.1718	0.0024
41,600	6.9691	0.3426	1.3559	0.1913	0.3881	0.0372
21,600	7.0636	0.3432				

2.3. Boundary conditions

Periodic boundaries are used for the inlet and outlet of the flow domain. Constant mass flow rate of air with 300 K ($Pr = 0.7$) is assumed in the flow direction rather than constant pressure drop due to periodic flow conditions. The inlet and outlet profiles for the velocities must be identical. The physical properties of the air have been assumed to remain constant at average bulk temperature. Impermeable boundary and no-slip wall conditions have been implemented over the channel walls as well as the baffle. The constant temperature of all the channel walls is maintained at 310 K while the baffle plate is assumed at conjugate wall (low thermal resistance) conditions.

3. Results and discussion

3.1. Verification of smooth square-channel

Verification of the heat transfer and friction factor of the smooth square-channel without baffle is performed by comparing with the previous values under a similar operating condition as shown in Fig. 2a and b, respectively. The present numerical smooth square-channel result is found to be in excellent agreement with exact solution values obtained from the open literature [34] for both the Nusselt number and the friction factor, less than ±0.5% deviation. The exact solutions of the Nusselt number and the friction factor for laminar flows over square channels with constant wall temperature are as follows [34]:

$$Nu_0 = 2.98 \tag{12}$$

$$f_0 = 57/Re \tag{13}$$

3.2. Flow structure

It is necessary to understand the flow structure and behavior in the baffled channel before discussing the results. The flow structure in the channel mounted periodically with various baffles on the lower and upper walls can be displayed by considering the streamline plots as depicted in Figs. 3–5 for the cases of 45° and 90° inline baffles, respectively. Here the velocity vectors and streamlines of the baffle modules are presented at $Re = 800$, BR = 0.2 and $s = 1$.

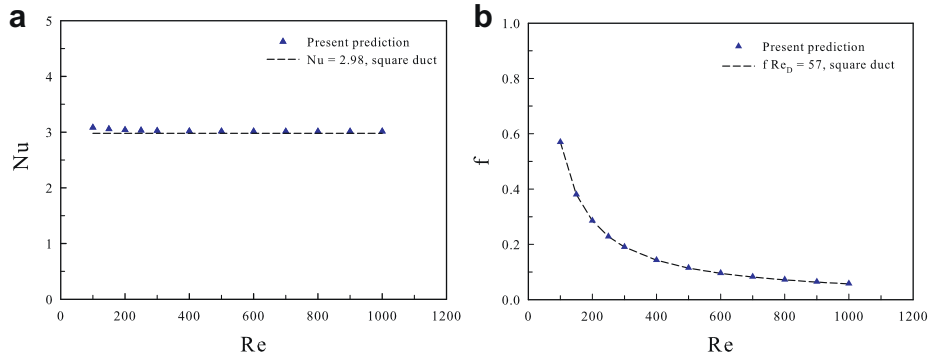

Fig. 2. Verification of (a) Nusselt number and (b) friction factor for smooth square-channel.

Fig. 3a and b shows, respectively, the streamlines in transverse planes at different locations with temperature maps superimposed and the iso-surfaces of $\lambda_2 = -250$ with velocity vectors superimposed, respectively. Fig. 4 presents streamlines with $\lambda_2 = -250$ iso-surfaces superimposed for the angled baffle in the lower wall. These are the most notable characteristics of the effects of the 45°-angled baffles on the mainstream flow. These effects are: mainstream flow separation, recirculation/vortex, and angled secondary flow. As the mainstream flow passes over the 45° inline baffles, it separates and creates recirculation or vortex flow behind the baffle due to high pressure difference across the angled baffle before moving helically along the baffle cavity (or the interbaffle spacing) and then rolling up. It is visible in Fig. 3a that two counter-rotating vortices or longitudinal vortex flows created by the 45° baffles appear on the upper and lower parts of the channel apart from four small vortices occurring at the four corners of the channel. In each of the two main vortex flows, the center of the main vortex flow (or vortex core) of the BLE plane, first plane in Fig. 3a, is at about the middle region of the cavity. When moving to the quarter baffle location, second plane in Fig. 3a, two vortex core centers appear: one, as mentioned in the first plane, in the upstream region of the baffle and the other in the downstream one. The upstream vortex core center is gradually vanishing and moves to the downstream one at the half baffle location as seen in third plane of Fig. 3a. Then, only the downstream one appears until it reaches the BTE of the baffle module (see fourth and fifth planes in Fig. 3a) and the vortex flow repeats itself as it gets to the BLE of the next module. The direction of the vortex core can be visualized by considering the iso-surfaces of $\lambda_2 = -250$ as can be seen in Fig. 3b. The appearance of two streamwise main vortex flows leads to relatively high heat transfer because of better flow mixing between the core and the wall regions as shown in Fig. 4. It is concluded that the presence of

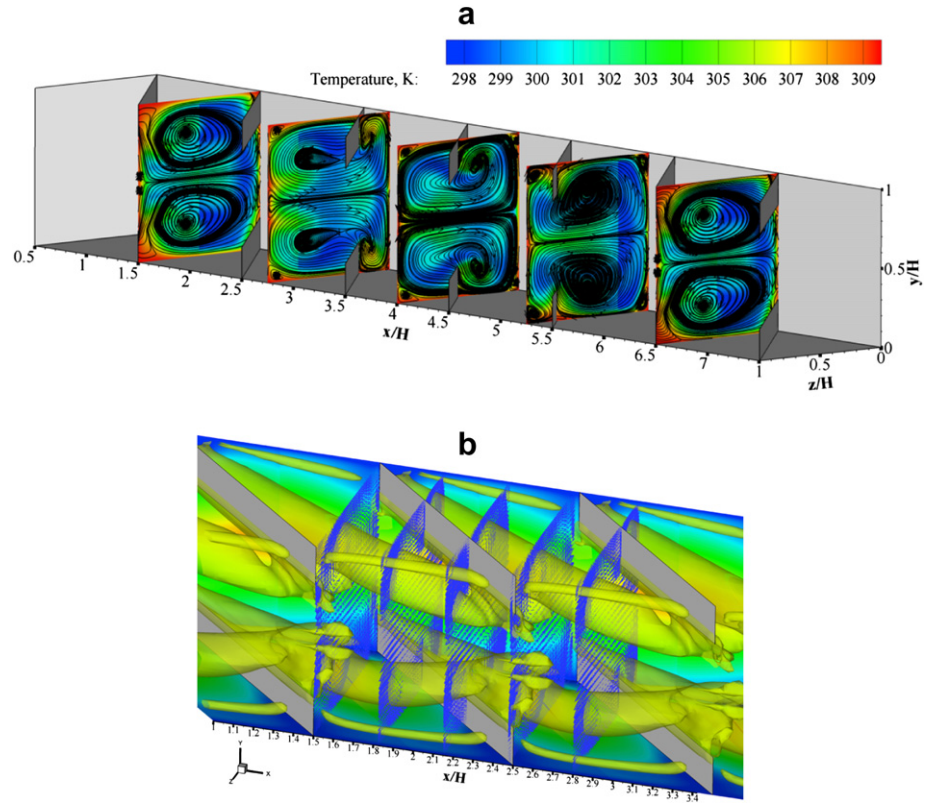

Fig. 3. (a) Streamlines in transverse planes and (b) iso-surface of $\lambda_2 = -250$ with velocity vectors superimposed for 45° inline baffles at $Re = 800$ and BR = 0.2.

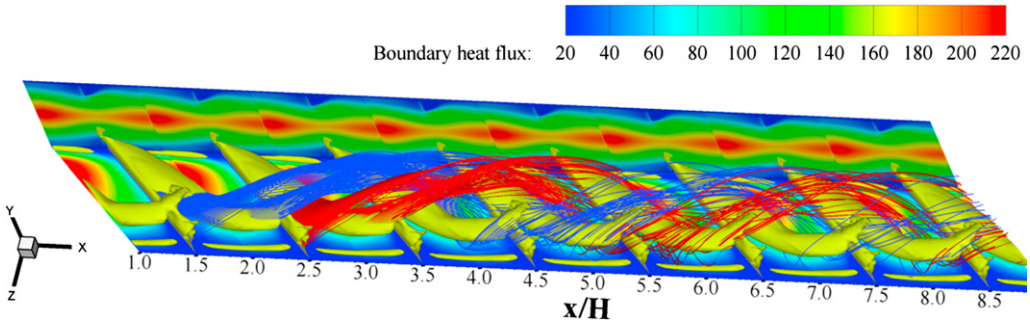

Fig. 4. Streamlines with $\lambda_2 = -250$ iso-surface superimposed for 45° inline lower baffles at $Re = 800$ and BR = 0.2.

the 45° baffles in inline arrangement creates two main counter-rotating vortices resulting in longer flow path and high strength of vortex due to changing in its orientation. For the 90° baffle case, only two transverse vortices are found and trapped behind each baffle as can be seen in Fig. 5 and this case is similar to previous work [9,13] and it will not be repeated here.

The plots of streamlines with wall heat fluxes superimposed showing the impingement flows on the lower wall and on the BLE sidewall of one module are shown in Fig. 6a and b, respectively. Fig. 7a and b also displays streamlines of multiple impinging jets on the lower wall and the BLE sidewall of several modules for the 45° inline baffle, respectively. In these figures, it can be observed that impinging jets occur periodically in a central area of the BLE sidewall cells and in a region on the lower wall in the cavity of consecutive baffles (also on the upper wall due to symmetry). A close examination reveals that the impinging jet on the BLE sidewall comes from the helical flows rolling up at the opposite side as seen in Fig. 7b. The helical vortex flow moves along the baffle cavity to the BTE sidewall and rolls up to impinge on the BLE sidewall, the upper or lower walls of the third or fourth module downstream. After impingement, the jet splits over the wall and recombines into two helical streams at the nearby baffle end (see Fig. 6) to create vortex flows again with shorter pitch lengths. The helical pitch length of the main vortex flow is about 3H–4H before impingement and becomes shorter after impingement. This means that the helical vortex flow passes over three or four baffle modules from a BTE side to the other BLE side before impingement. This behavior is identical on both the upper and lower parts so two streamwise vortices with non-uniform helical pitch length form in the channel. It can be concluded that a pair of twisted vortex (P-vortex) flows with non-uniform helical pitches created by the inclined baffles placed periodically can induce two impingement flows: one on the wall in the baffle cavity and the other on the BLE sidewall or P-vortex induced impingements for two walls can occur periodically in a flow through the angled baffle.

3.3. Heat transfer

Fig. 8a and b displays the contour plots of temperature field for the 45° baffle at Re = 800 and BR = 0.2 in (a) streamwise and (b) transverse planes, respectively. The figures show that there is a major change in the temperature field over the channel. This means that the P-vortex flows provide a significant influence on the temperature field, because it can induce better fluid mixing

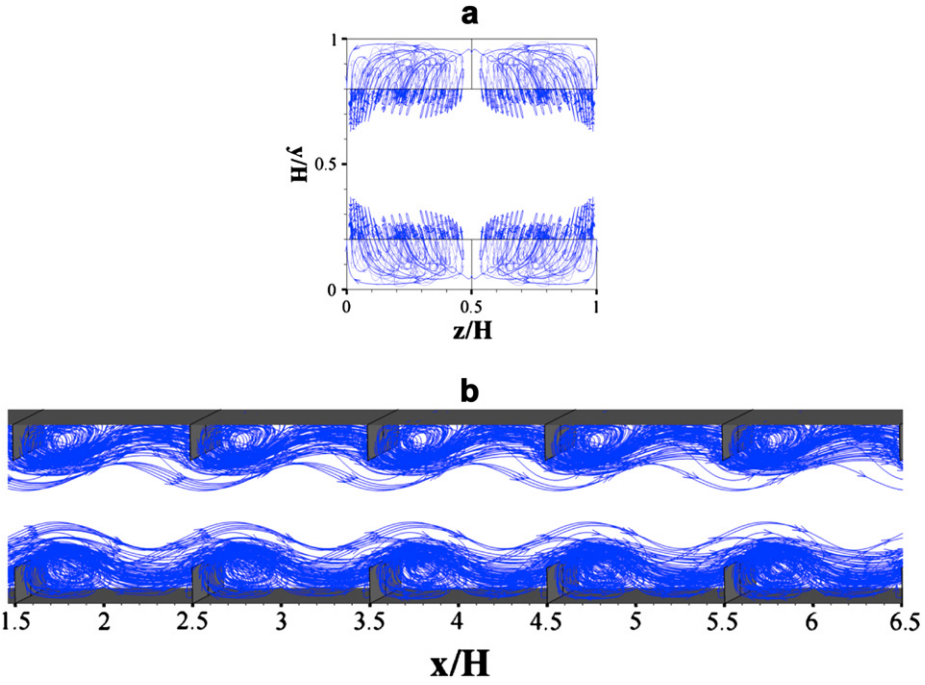

Fig. 5. Streamlines for 90° inline baffles; (a) front (view from upstream side) and (b) side views at $Re = 800$ and BR = 0.2.

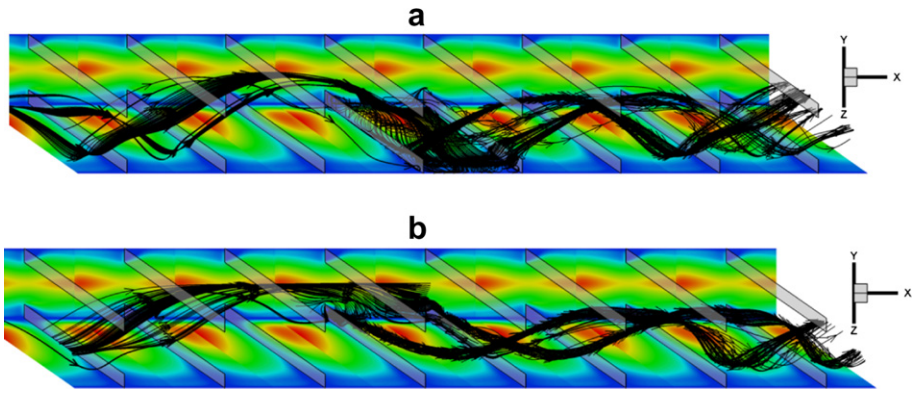

Fig. 6. Streamlines of impinging jet on (a) lower and (b) BLE sidewalls of one cell for 45° inline baffles at $Re = 800$ and BR = 0.2.

between the wall and the core flow regions, leading to a high temperature gradient over the heating channel wall. The higher temperature gradient can be observed where the flow impinges the channel walls while the lower one is found at the BTE sidewall area where the temperature in this region is somewhat high. However, the temperature field for this case is seen to be almost distributed uniformly in the entire flow in comparison with the 90° baffle case that will be mentioned next.

The contour plots of temperature field for the 90° baffle at $Re = 800$ and BR = 0.2 in (a) streamwise and (b) transverse planes are depicted in Fig. 9a and b, respectively. In these figures, a major change in the temperature field is found only in the regime within the baffle cavity while in the region of the baffle tip (core flow), there is a minor change. This implies that the transverse recirculation zone downstream of the baffle provides a significant influence on the temperature field only in this zone while the core flow in the opposite baffle tips is not affected by the presence of the 90° baffle. The higher temperature gradient can be observed only in the middle region of the baffle cavities where the flow impinges the channel walls. The lower one can be found in the area around the baffle.

Local Nu_x contours for the channel walls with the 45° and the 90° inline baffles at Re = 800 and BR = 0.2 are presented in Fig. 10a and b, respectively. In these figures, it appears that the higher Nu_x values over the walls with the 45° baffle are seen in a larger area, except for a small region in the corner of the BTE, in comparison with the 90° baffle case. The peaks are observed at the impingement areas on the BLE sidewall and walls of the baffle cavities for the 45° baffle but on the sidewalls only for the 90° baffle. The peak Nu_x value for the 45° baffle is found to be about 3 times above that for the 90° baffle. This indicates a merit of employing the 45° baffle over the smooth channel or the 90° baffle for enhancing heat transfer.

The variation of the average Nu/Nu_0 ratio with Reynolds number for various baffles at different BRs is depicted in Fig. 11a while that for different wall surfaces of the 45° inline baffle case is shown in

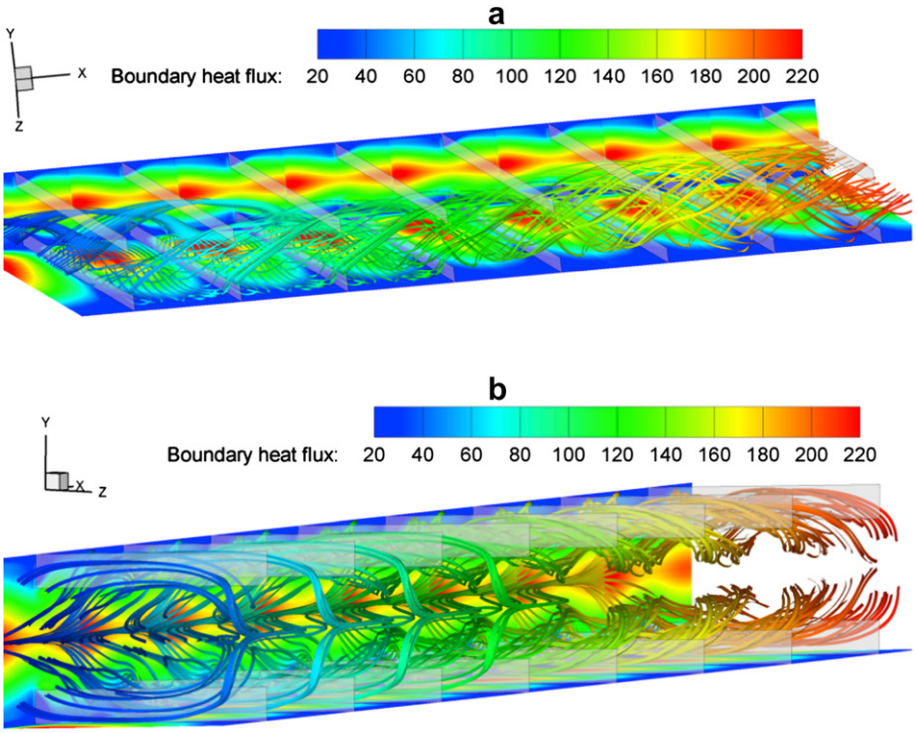

Fig. 7. Streamlines of impinging jets on (a) lower wall and (b) BLE sidewall of several cells for 45° inline baffles at $Re = 800$ and BR = 0.2.

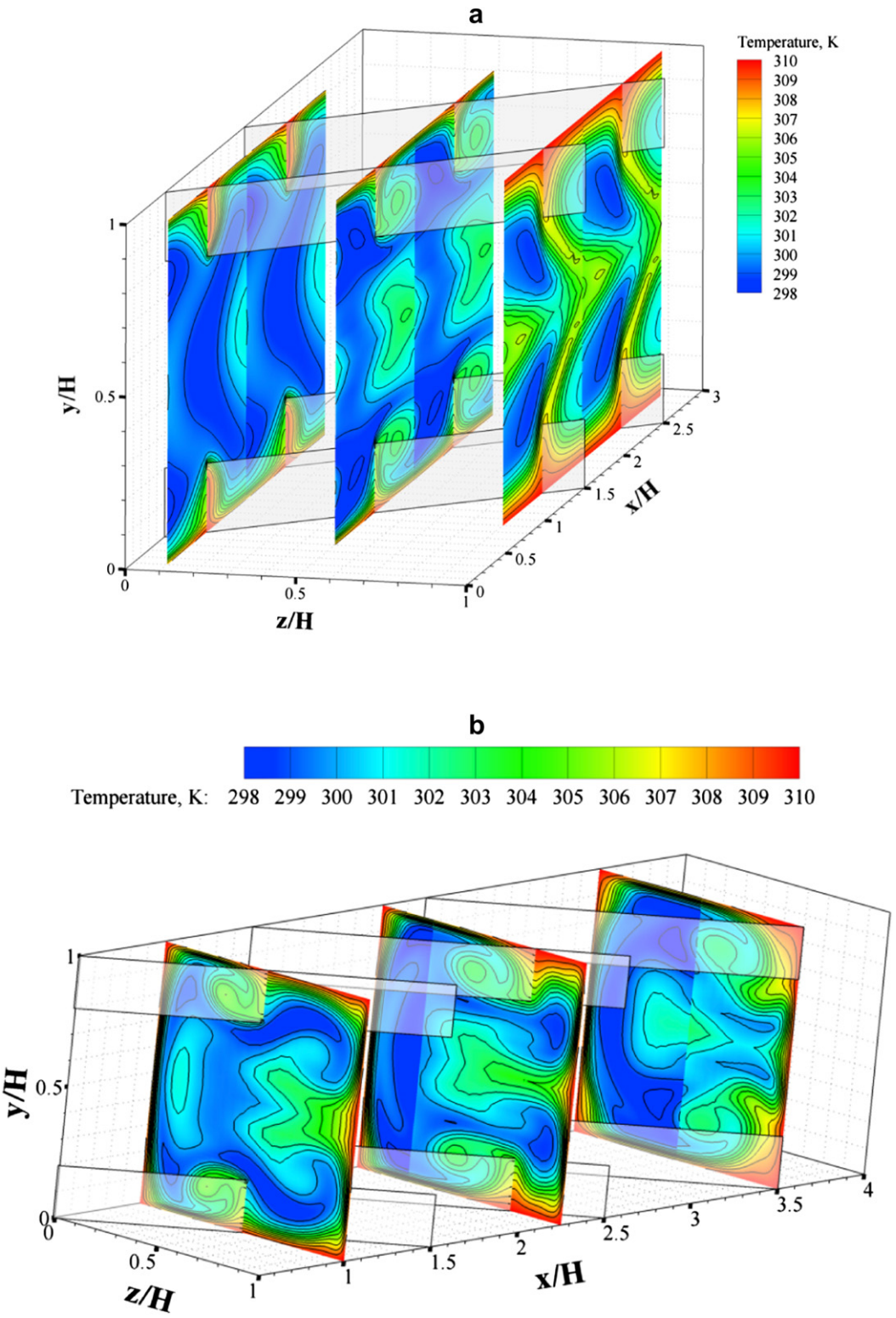

Fig. 8. Temperature contours for 45° inline baffles in (a) streamwise and (b) transverse planes, at $Re = 800$ and BR = 0.2.

Fig. 11b. It is worth noting in Fig. 11a that the Nu/Nu_0 value tends to increase with the rise of Reynolds number for all BR values. The higher BR value results in the increase in the Nu/Nu_0 value. The 45° staggered and inline baffles perform nearly the same and much better than the 90° baffle for augmenting heat transfer. The 45° staggered baffle yields slightly higher Nu/Nu_0 value than the 45° inline baffle only for the case of BR $\geq$ 0.25. The Nu value for both the 45° baffles with BR = 0.3 is found to be about 100% over that for the 90° baffle. Thus, the generation of P-vortex flows from using the 45° baffles as well as the role of better fluid mixing and the impingement is the main reason for the augmentation in heat transfer of the channel. In addition, it can be noted that the 45° baffles with

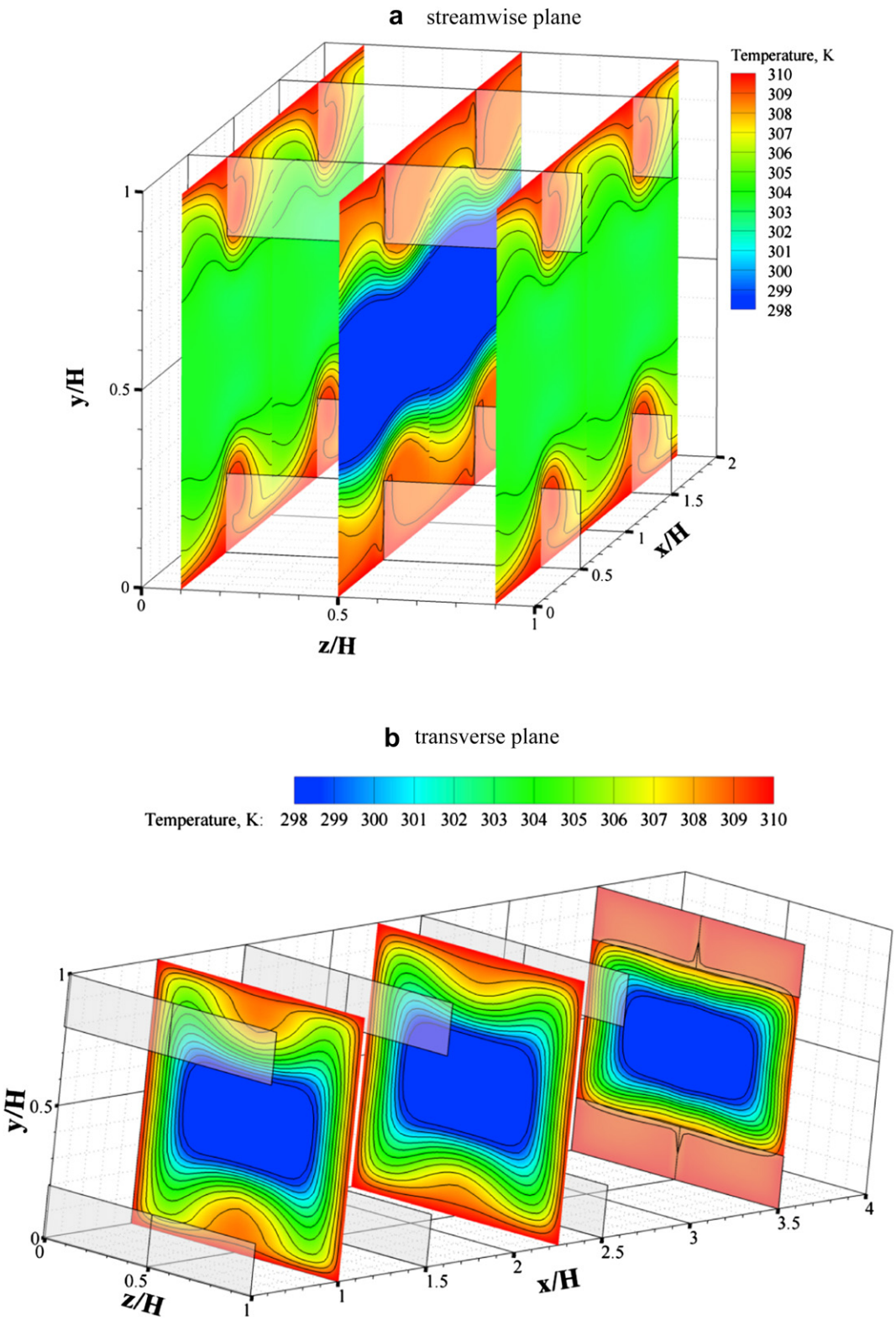

Fig. 9. Temperature contours for 90° inline baffles in (a) streamwise and (b) transverse planes, at $Re = 800$ and BR = 0.2.

BR $\geq$ 0.15 perform more efficiently than the 90° baffle with BR = 0.3 for all Re values. This indicates that the strength of vortex induced by the 45° baffle with lower BR value is strong enough to yield a mixing intensity of flow between the wall and the core. The scrutiny of Fig. 11a reveals that the 45° baffle with the BR range studied yields heat transfer rate of about 1.5–8.5 times higher than the smooth channel with no baffle.

In Fig. 11b, it is found that the heat transfer on the BLE sidewall for the 45° inline baffle with BR $\geq$ 0.2 is about 50% higher than that on the upper wall for one with BR = 0.3 while the heat transfer on

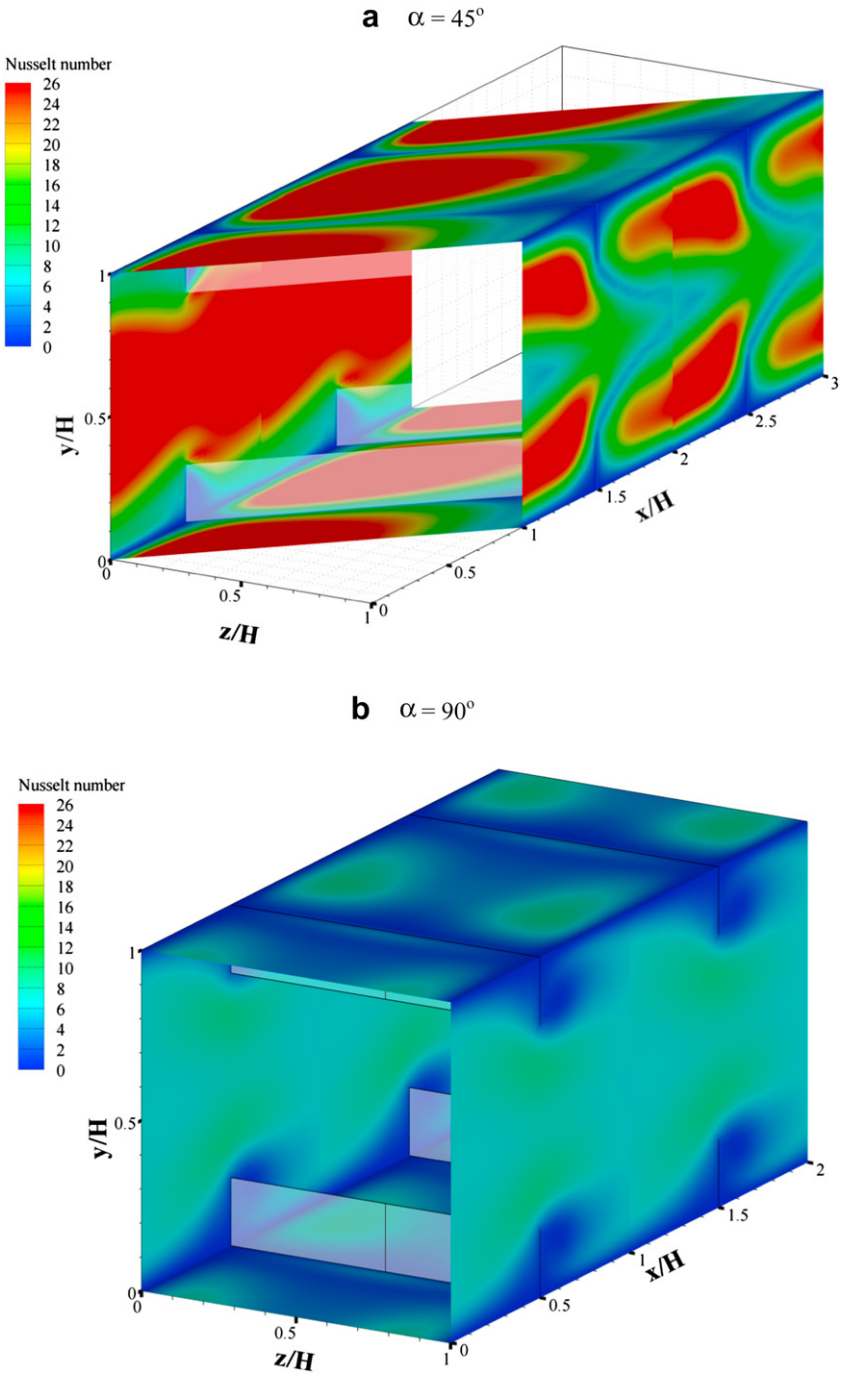

Fig. 10. Nu_x contours for (a) 45° and (b) 90° inline baffles at $Re = 800$ and BR = 0.2.

the BTE sidewall is seen to be the lowest. This can be attributed to the impingement flow effect induced by stronger P-vortex flows on the BLE sidewall.

3.4. Pressure loss

In general, the heat transfer augmentation is concerned with penalty in terms of increased friction coefficient resulting in higher pressure drop. Fig. 12 presents the variation of the normalized friction factor, f/f_0 with Reynolds number values for various baffles and BRs. In the figure, it is noted that the f/f_0 tends to increase with the rise of Reynolds number and BR values for all baffles. The use of the 90° baffle leads to extreme increase in friction factor in comparison with the plain channel with no baffle. For baffles, the decrease in the BR value gives rise to the reduction in friction factor. The friction factor for both the 45° baffles appears to be about 10–150% less than that for the 90° baffle depending on the BR values. This shows a merit of using the 45° baffles in stead of the 90° baffle for pressure loss reduction. The 45° staggered baffle also provides slightly higher friction factor than the 45° inline baffle only for BR $\geq$ 0.20 while for BR $\leq$ 0.15, both the 45° baffles give similar results. The f/f_0 value for both the 45° baffle is found to be about 2–70 times over the plain channel depending on the BR and Reynolds number values.

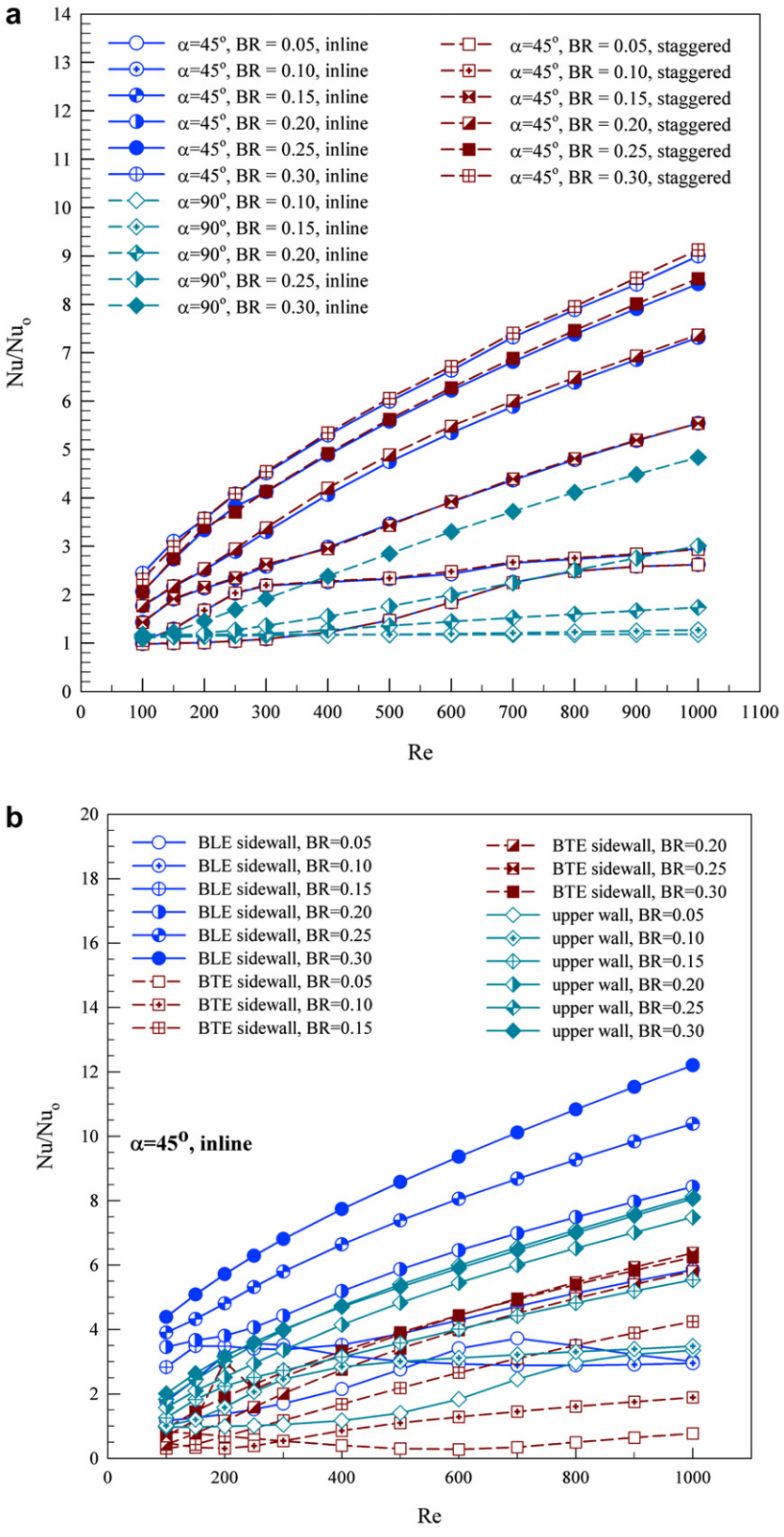

Fig. 11. Variation of Nu/Nu_0 with Reynolds number for (a) various baffles and (b) various walls.

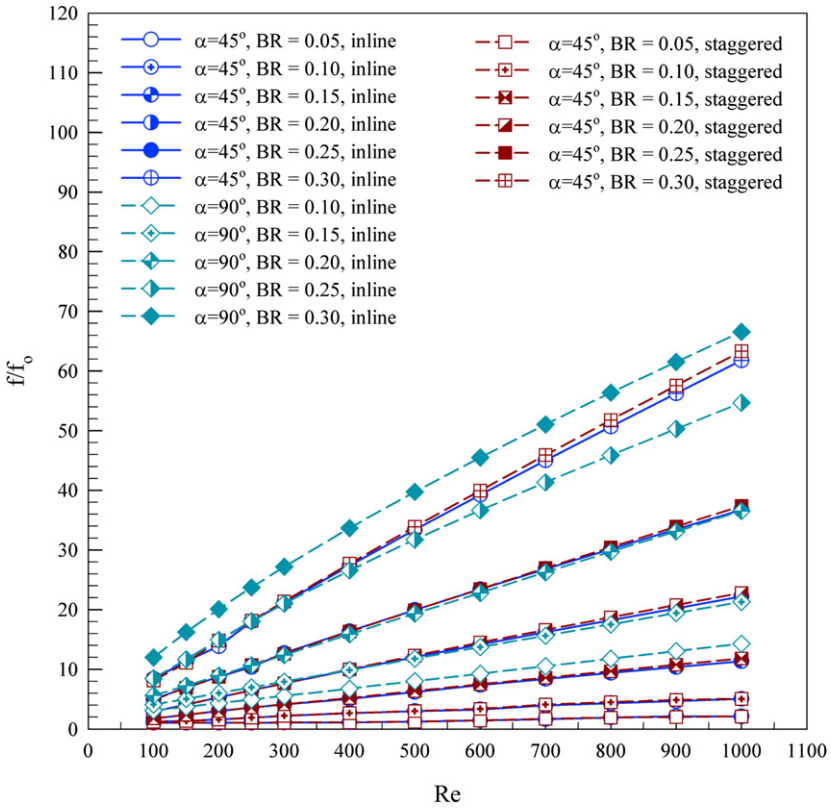

Fig. 12. Variation of f/f_0 with Reynolds number for baffles at various BRs.

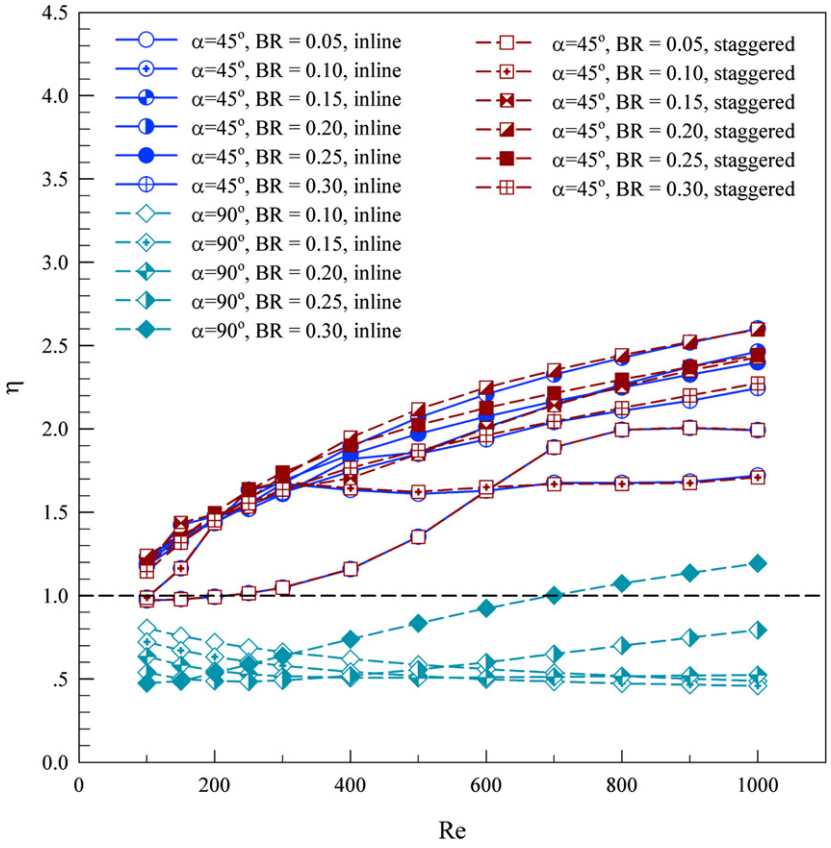

Fig. 13. Comparison of thermal enhancement factor for baffles at various BRs.

3.5. Performance evaluation

Fig. 13 exhibits the variation of thermal enhancement factor (η) for air flowing in the baffled square channel. In the figure, the enhancement factor of both the 45° baffles tends to increase with the rise of Reynolds number and BR values while shows a uniform trend at BR = 0.1 and $Re > 300$ or at BR = 0.05 and $Re > 700$. Both the 45° baffles provide the highest enhancement factor while the 90° baffle yields the lowest. The enhancement factor for the 90° baffle with all BRs is found to be lower than unity except for the case of BR = 0.3 and $Re > 700$, indicating that this case are not advantageous with respect to smooth channel with no baffle. This is a reason why the 90° baffle is not much used to enhance heat transfer in many thermal engineering applications in comparison with other turbulators. The enhancement factors of both the 45° baffles are seen to be above unity for all BRs and vary between 1.0 and 2.6, depending on the BR and Re values. For the results investigated, the 45° baffles with BR = 0.2 gives the best thermal enhancement factor and one with BR = 0.25 yields slightly lower. This suggests that to obtain high thermal performance, the 45° baffles with BR = 0.2–0.25 should be applied.

4. Conclusions

Laminar periodic flow and heat transfer characteristics in a square channel fitted with 90° transverse and 45° inclined baffle elements in tandem, inline and staggered arrangements on two opposite walls have been investigated numerically. The P-vortex flows created by using the 45° baffles help to induce impingement flows on the BLE sidewall and wall in the baffle cavity leading to drastic increase in heat transfer in the square channel. The order of enhancement is about 150–850% for using both the 45° baffles with BR = 0.05–0.3. However, the heat transfer augmentation is associated with enlarged pressure loss ranging from 2 to 70 times above the smooth channel. Thermal enhancement factors for both the 45° baffle arrays are found to be almost the same and much higher than unity and theirs maximum values are about 2.6 indicating higher thermal performance over the smooth channel. For the 45° baffles, the heat transfer enhancement is around 100–200% higher than that for the 90° baffle whereas the friction loss can be reduced at about 10–150%.

Acknowledgement

The author would like to acknowledge with appreciation, the Thailand Research Fund (TRF) for the financial support.

References

[1] S.V. Patankar, C.H. Liu, E.M. Sparrow, Fully developed flow and heat transfer in ducts having streamwise-periodic variations of cross-sectional area. ASME J. Heat Transfer 99 (1977) 180–186.
[2] C. Berner, F. Durst, D.M. McEligot, Flow around baffles. Trans. ASME J. Heat Transfer 106 (1984) 743–749.
[3] B.W. Webb, S. Ramadhyani, Conjugate heat transfer in a channel with staggered ribs. Int. J. Heat Mass Transfer 28 (1985) 1679–1687.
[4] K.M. Kelkar, S.V. Patankar, Numerical prediction of flow and heat transfer in a parallel plate channel with staggered fins. ASME J. Heat Transfer 109 (1987) 25–30.
[5] C.H. Cheng, W.H. Huang, Laminar forced convection flows in horizontal channels with transverse fins placed in entrance regions. Int. J. Heat Mass Transfer 20 (1991) 1315–1324.
[6] C.H. Cheng, W.H. Huang, Numerical prediction for laminar forced convection in parallel-plate channels with transverse fin arrays. Int. J. Heat Mass Transfer 34 (11) (1991) 2739–2749.
[7] M.A. Habib, A.M. Mobarak, M.A. Sallak, E.A. Abdel Hadi, R.I. Affify, Experimental investigation of heat transfer and flow over baffles of different heights. ASME J. Heat Transfer 116 (1994) 363–368.
[8] A. Amiri, K. Vafai, T.M. Kuzay, Effects of boundary conditions on non-Darcian heat transfer through porous media and experimental comparison. Numer. Heat Transfer, Part A: Appl. 27 (1995) 651–664.
[9] J.R. Lopez, N.K. Anand, L.S. Fletcher, Heat transfer in a three-dimensional channel with baffles. Numer. Heat Transfer, Part A: Appl. 30 (1996) 189–205.
[10] Z. Guo, N.K. Anand, Three-dimensional heat transfer in a channel with a baffle in the entrance region. Numer. Heat Transfer, Part A: Appl. 31 (1) (1997) 21–35.
[11] Y.T. Yang, C.Z. Hwang, Calculation of turbulent flow and heat transfer in a porous-baffled channel. Int. J. Heat Mass Transfer 46 (2003) 771–780.
[12] B.M. Da Silva Miranda, N.K. Anand, Convective heat transfer in a channel with porous baffles. Numer. Heat Transfer, Part A: Appl. 46 (5) (2004) 425–452.
[13] N.B. Santos, M.J.S. De Lemos, Flow and heat transfer in a parallel-plate channel with porous and solid baffles. Numer. Heat Transfer, Part A: Appl. 49 (5) (2006) 471–494.
[14] K.H. Ko, N.K. Anand, Use of porous baffles to enhance heat transfer in a rectangular channel. Int. J. Heat Mass Transfer 46 (2003) 4191–4199.
[15] S.S. Mousavi, K. Hooman, Heat and fluid flow in entrance region of a channel with staggered baffles. Energy Convers. Manage. 47 (2006) 2011–2019.
[16] Y.L. Tsay, J.C. Cheng, T.S. Chang, Enhancement of heat transfer from surface-mounted block heat sources in a duct with baffles. Numer. Heat Transfer, Part A: Appl. 43 (8) (2003) 827–841.
[17] S. Sripattanapipat, P. Promvonge, Numerical analysis of laminar heat transfer in a channel with diamond-shaped baffles. Int. Commun. Heat Mass Transfer 36 (1) (2009) 32–38.
[18] P. Promvonge, S. Sripattanapipat, S. Tamna, S. Kwankaomeng, C. Thianpong, Numerical investigation of laminar heat transfer in a square channel with 45° inclined baffles Int. Commun. Heat Mass Transfer 37 (2) (2010) 170–177.
[19] J.C. Han, Y.M. Zhang, C.P. Lee, Augmented heat transfer in square channels with parallel, crossed and V-shaped angled ribs. ASME J. Heat Transfer 113 (1991) 590–596.
[20] J.C. Han, Y.M. Zhang, C.P. Lee, Influence of surface heat flux ratio on heat transfer augmentation in square channels with parallel, crossed, and V-shaped angled ribs. ASME J. Turbomach. 114 (1992) 872–880.
[21] T.M. Liou, J.J. Hwang, Turbulent heat transfers augmentation and friction in periodic fully developed channel flows. ASME J. Heat Transfer 114 (1992) 56–64.
[22] T.M. Liou, J.J. Hwang, Effect of ridge shapes on turbulent heat transfer and friction in a rectangular channel. Int. J. Heat Mass Transfer 36 (1993) 931–940.
[23] M.E. Taslim, T. Li, D.M. Kercher, Experimental heat transfer and friction in channels roughened with angled, V-shaped, and discrete ribs on two opposite walls. ASME J. Turbomach. 118 (1996) 20–28.
[24] A. Murata, S. Mochizuki, Comparison between laminar and turbulent heat transfer in a stationary square duct with transverse or angled rib turbulators. Int. J. Heat Mass Transfer 44 (2001) 1127–1141.
[25] P.R. Chandra, C.R. Alexander, J.C. Han, Heat transfer and friction behaviour in rectangular channels with varying number of ribbed walls. Int. J. Heat Mass Transfer 46 (2003) 481–495.
[26] G. Tanda, Heat transfer in rectangular channel with transverse and V-shaped broken ribs. Int. J. Heat Mass Transfer 47 (2004) 229–243.
[27] P. Promvonge, C. Thianpong, Thermal performance assessment of turbulent channel flow over different shape ribs. Int. Commun. Heat Mass Transfer 35 (10) (2008) 1327–1334.
[28] V.S. Hans, R.P. Saini, J.S. Saini, Performance of artificially roughened solar air heaters – a review. Renewable Sustainable Energy Rev. 13 (2009) 1854–1869.
[29] R.P. Varun, S.K. SainiSingal, A review on roughness geometry used in solar air heaters. Sol. Energy 81 (2007) 1340–1350.
[30] S.V. Patankar, Numerical Heat Transfer and Fluid Flow. McGraw-Hill, New York, 1980.
[31] J. Jeong, F. Hussain, On the identification of a vortex. J. Fluid Mech. 285 (1995) 69–94.
[32] P.J. Roache, Verification and Validation in Computational Science and Engineering. Hermosa Publishers, Albuquerque, NM, 1998, ISBN 0913478083.
[33] I. Celik, U. Ghia, P.J. Roache, C.J. Freitas, H. Coleman, P.E. Raad, Procedure for estimation and reporting of uncertainty due to discretization in CFD applications. ASME J. Fluids Eng. 130 (2008) 078001–078004.
[34] F. Incropera, P.D. Dewitt, Introduction to Heat Transfer, fifth ed. John Wiley & Sons Inc, 2006.